Journal of ELECTRONIC MATERIALS, Vol. 45, No. 3, 2016
DOI: 10.1007/s11664-015-4063-3

Thermoelectric Properties of the α-As_2Te_3 Crystalline Phase

J.-B. VANEY,[1,2,6] J. CARREAUD,[2] G. DELAIZIR,[2] C. MORIN,[3] J. MONNIER,[3] E. ALLENO,[3] A. PIARRISTEGUY,[4] A. PRADEL,[4] A.P. GONÇALVES,[5] E.B. LOPES,[5] C. CANDOLFI,[1] A. DAUSCHER,[1] and B. LENOIR[1]

1.—Institut Jean Lamour (IJL), UMR 7198 CNRS-Université de Lorraine, Nancy, France. 2.—SPCTS, Université de Limoges UMR CNRS 7315, Limoges, France. 3.—Institut de Chimie et des Matériaux de Paris Est (ICMPE), UMR 7182 CNRS, CMTR, Thiais, France. 4.—Institut Charles Gerhardt (ICG), UMR 5253 CNRS-Université Montpellier 2, Montpellier, France. 5.—C2TN Instituto Superior Técnico, Universidade de Lisboa, 2695-066 Bobadela, LRS, Portugal. 6.—e-mail: jean-baptiste.vaney@univ-lorraine.fr

As_2Te_3 exists in two crystallographic configurations: α- and β-As_2Te_3, of which only the latter crystallizes in the same rhombohedral structure-type as Bi_2Te_3. While β-As_2Te_3 shows interesting thermoelectric (TE) properties which can be adjusted through alloying, the transport properties of the monoclinic phase α-As_2Te_3, more thermodynamically stable than the β-phase at room temperature, has not yet been studied thoroughly. We report here on the samples preparation by powder metallurgy, and on the microstructural characterization of polycrystalline α-As_2Te_3. Preliminary results on the electrical and thermal properties measured between 5 K and 523 K are also reported. Transport properties measurements were performed both along and perpendicular to the pressing direction indicating that the transport properties demonstrate some degree of anisotropy. Remarkably, low thermal conductivity values (below 1 W m^{-1} K^{-1} above 300 K) were measured suggesting that this compound may be an interesting platform to design novel TE materials with high efficiency.

Key words: Arsenic telluride, thermoelectric materials, high- and low-temperature thermoelectric properties, crystal structure

INTRODUCTION

Thermoelectric (TE) materials offer an effective way to convert thermal energy into electrical energy (Seebeck effect) and, reciprocally, electrical energy into thermal energy (Peltier effect). The performance of TE devices is directly related to the properties of the materials through the dimensionless TE figure-of-merit, ZT, defined by $ZT = \frac{\sigma T \alpha^2}{\lambda} = \frac{PT}{\lambda}$ where T is the absolute temperature, α is the Seebeck coefficient (or thermopower), $P = \alpha^2/\rho$ is the power factor, ρ is the electrical resistivity and λ is the total thermal conductivity. For decades, the performance of TE materials have been limited, confining them to niche applications and markets.[1] Owing to strong interdependence between the three transport properties, achieving high ZT on a broad temperature range still remains the most challenging aspect in thermoelectricity.[2,3]

Recently, the metastable β-As_2Te_3 phase, isostructural to the state-of-the art Bi_2Te_3-based materials, showed an interesting performance upon substitution of Sn for As, with peak ZT around 0.6 at 423 K.[4] However, As_2Te_3 exists in two crystallographic forms: the rhombohedral β-As_2Te_3, which was first obtained at high pressure[5] and then directly synthesized by rapid quenching from the melt,[6,7] and the monoclinic α-As_2Te_3.[8] The former transforms into the latter upon heating above 410 K. α-As_2Te_3 has been scarcely studied from the TE point of view but may show interesting properties at which early studies[9,10] and first-principles calculations hint.[11]

(Received June 2, 2015; accepted September 15, 2015; published online September 30, 2015)

Here, we describe the crystalline structure of α-As_2Te_3 and its successful synthesis and shaping by the spark plasma sintering (SPS) technique. The TE properties of this binary compound are discussed between 5 K and 523 K. Although the maximum ZT remains very low, our results suggest that there is still much room for further improvement upon alloying if the carrier concentration can be properly controlled.

EXPERIMENTAL

The α-As_2Te_3 sample was prepared by direct reaction of stoichiometric amounts of pure elements [As (Goodfellow, 99.99%, shots) and Te (5 N+, 99.999%, shots)] sealed under secondary vacuum (5×10^{-6} mbar) in quartz tubes. The tubes were heated slowly up to 923 K at a rate of 10 K min^{-1}, dwelt at this temperature for 2 h, and finally quenched in an ice–water mixture. At this step, the β-phase was obtained.[4] The ingot was subsequently annealed at 613 K for 3 days to finally obtain the pure α-As_2Te_3 phase. The resulting ingots were ground into micron-sized powders and consolidated by SPS into a 10-mm-diameter cylindrical pellet under a pressure of 50 MPa at a temperature of 613 K for 2 min. The obtained pellet showed a relative density close to 99% of the theoretical density.

The crystal structure was determined by powder x-ray diffraction (PXRD) at 300 K with a Bruker D8 Advance instrument using CuKα_1 radiation. The chemical homogeneity of the sample was checked by scanning electron microscopy (SEM) and energy dispersive x-ray spectroscopy (EDXS) using a Quanta FEG FEI. Electron probe micro-analysis (EPMA) was performed with a JEOL JXA 8530F equipped with wavelength-dispersive spectrometers. Backscattered electrons were used for imaging the surface of the samples. In order to minimize matrix effects, x-ray intensities of As and Te were compared with those of a calibrated β-As_2Te_3 standard for quantitative analysis. The chemical compositions of the α-As_2Te_3 specimens were determined from the analysis of a set of at least 90 different points for each sample. Bulk pieces of the densified sample were carefully polished down to 1-μm alumina powder for EPMA analysis.

The TE properties were measured between 5 K and 523 K on well-shaped samples cut with a diamond wire-saw (typical dimensions of $2 \times 3 \times 6$–8 mm^3). Owing to the anisotropic crystal structure of the present compound, the transport properties were measured on samples cut both parallel and perpendicular to the pressing direction. α and ρ data were collected in the 300 K–523 K temperature range using a ZEM-3 apparatus (ULVAC-RIKO). Thermal diffusivity a was measured by a laser flash technique (Netzsch LFA 427) between 300 K and 523 K. The specific heat, C_p, was measured by differential scanning calorimetry (DSC Netzsch Pegasus) above room temperature. The thermal conductivity was then calculated via $\kappa = a\ C_p\ d$ where d is the density measured using the mass and the geometric dimensions of the densified pellet. The density was considered temperature-independent in the present case. The errors for each measured properties are estimated to be about 5% so that the combined uncertainty on the ZT values is at most ~20%. To measure the TE properties between 5 K and 300 K, we used the thermal transport option (TTO) of a physical property measurement system (PPMS; Quantum Design). These measurements were conducted by brazing four copper bars on the samples to ensure excellent electrical and thermal contacts. Specific heat was measured on a small prism-shaped sample (mass of ~15 mg) from 2 K to 260 K using the He^4 option of the PPMS.

RESULTS AND DISCUSSION

Structural and Chemical Characterizations

The study of α-As_2Te_3 is to be put in perspective with its counterpart β-As_2Te_3. The metastable β-As_2Te_3 (space group $R\bar{3}m$), produced by rapid quenching[6] or under high pressures,[7] transforms into the α structure (space group C2/m) upon heating above 410 K.[12] The perspective views of the unit cell of both structures (the hexagonal cell of β-As_2Te_3 is displayed rather than the rhombohedral cell) are represented on Fig. 1. It could be expected that both are very close and that the α form would appear as a distorted version of the more ordered β-structure. Projections of the atomic arrangements of the α- and β-phases along their respective a-axis

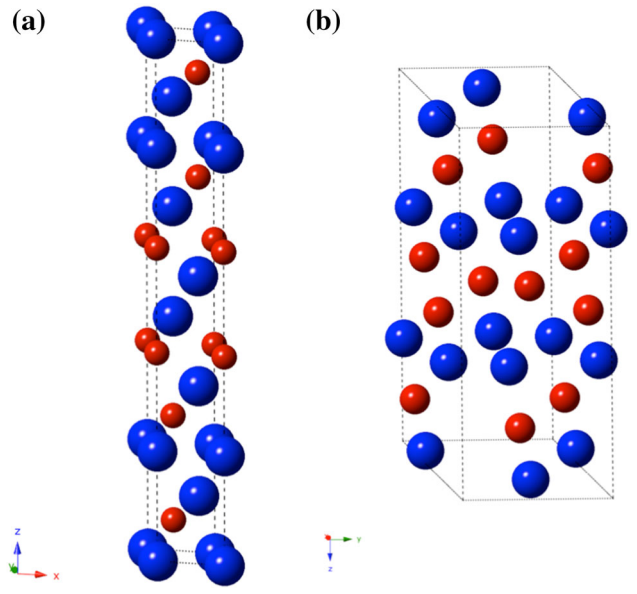

Fig. 1. Perspective view of the hexagonal crystal structure β-As_2Te_3 (rhombohedral of space group $R\bar{3}m$, a = 4.0473 Å and c = 29.5018 Å) (a) and α-As_2Te_3 (monoclinic of space group C2/m, a = 14.339, b = 4.0114, c = 9.8859, β = 95.046) (b). The As atoms are represented as small red balls and the Te atoms by large blue balls (Color figure online).

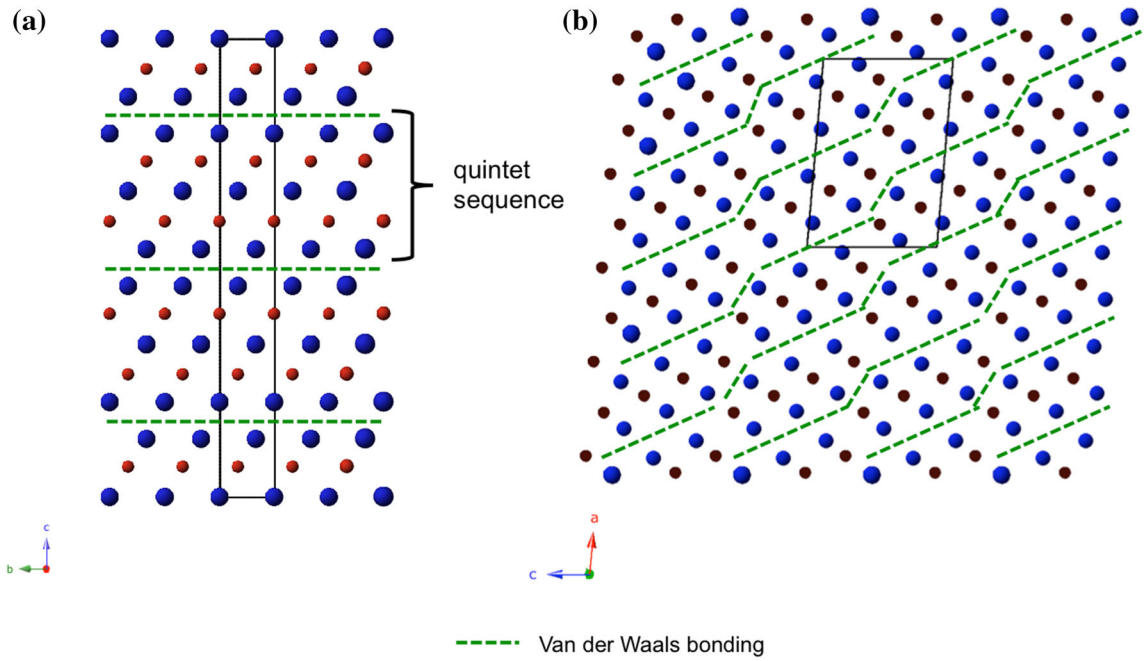

Fig. 2. Projections on to the *a*-axis of supercells of β-As_2Te_3 (a) and α-As_2Te_3 (b). The unit cells are represented by black lines, the As atoms are represented as small red balls and the Te atoms by large blue balls. The atomic plans alternation is in fact very different between the two structures. Van der Waals bonding is represented by the broken green lines (Color figure online).

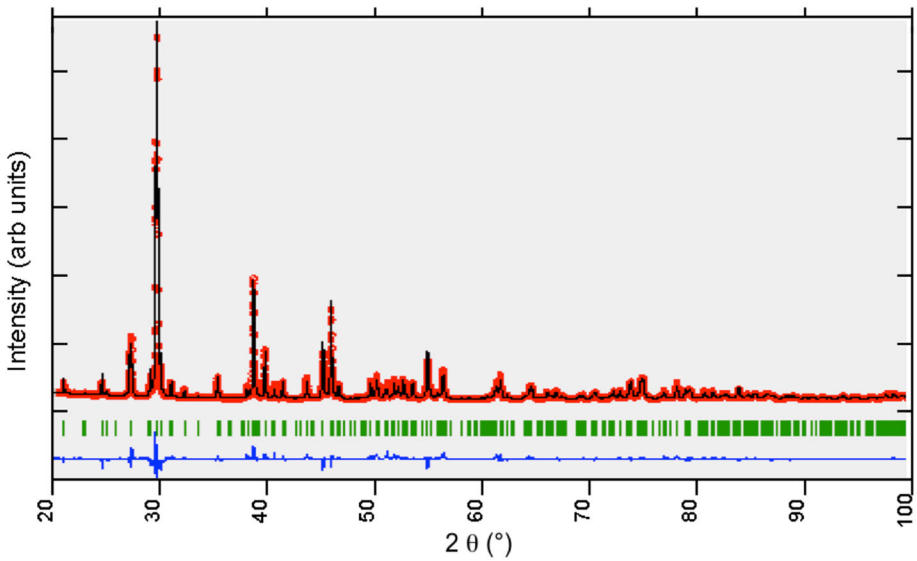

Fig. 3. Powder x-ray diffraction pattern of α-As_2Te_3. The observed data are marked as open red circles. The calculated profile is represented by a solid black line while the difference between experimental and numerical patterns is shown by the solid blue line (RF = 4.024, χ^2 = 8.04). The positions of the Bragg reflections are indicated as green bars (Color figure online).

are displayed in Fig. 2. It can be clearly observed that both show layered arrangements with alternating As-planes and Te-planes. However, upon closer examination, these projections reveal different sequences separated by van der Waals bonding with a quintet sequence Te_1-As-Te_2-As-Te_1 for β-As_2Te_3 in the *c*-direction and a zigzag stacking for the α-As_2Te_3 structure.[13]

Figure 3 presents the PXRD pattern collected on the binary sample α-As_2Te_3. All reflections can be indexed to the C2/m space group without any additional peak that would reveal a secondary phase. Due to the anisotropy of the structure, the sample shows a slight preferred orientation resulting in a very shallow renormalization of the relative intensities of the Bragg peaks. The Rietveld refinement of this pattern leads to good fit allowing the precise determination of the lattice parameters, in good agreement with literature data.[7] All refined parameters are described in Table I. SEM and x-ray

Table I. Refined lattice and atomic parameters for α-As_2Te_3 phase obtained from powder x-ray diffraction at room temperature

a **(Å)**	***b*** **(Å)**	***c*** **(Å)**	***β*** **(°)**
14.3392 ± 0.0004	4.0147 ± 0.0001	9.8859 ± 0.0003	95.046 ± 0.001
Atomic position	***x***	***y***	***z***
As_1	0.6135 ± 0.0004	0.0000	0.4406 ± 0.0006
As_2	0.2014 ± 0.0005	0.0000	0.1413 ± 0.0008
Te_1	0.2906 ± 0.0003	0.0000	0.2887 ± 0.0004
Te_2	0.7779 ± 0.0003	0.0000	0.3401 ± 0.0004
Te_3	0.3753 ± 0.0003	0.0000	0.0360 ± 0.0004
Reliability factors	R_{WP}	R_{Bragg}	χ^2
	11.41	4.024	8.04

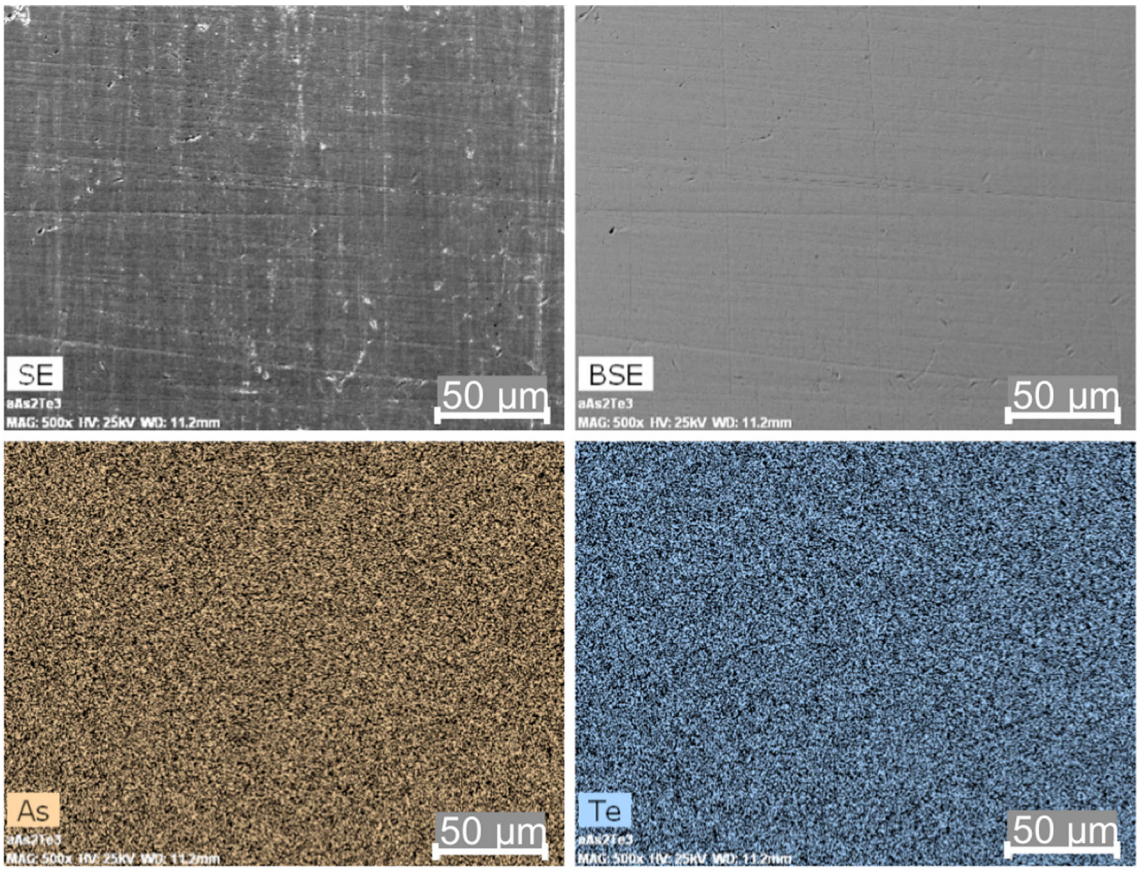

Fig. 4. Scanning electron microscope (SEM) elemental contrast picture of the sample α-As_2Te_3 in secondary electron (*SE*) and back-scattered electrons (*BSE*) mode, together with the corresponding element mapping of *As* and *Te*. The distribution of the elements is overall homogeneous.

mapping further revealed an overall homogeneous distribution of the different elements as displayed on Fig. 4. EPMA gave an average composition of $As_{1.99}Te_{3.01}$ for the compound, close to the nominal composition.

Thermoelectric Properties of the Binary Phase α-As_2Te_3

The temperature dependences of ρ and α measured parallel and perpendicular to the pressing

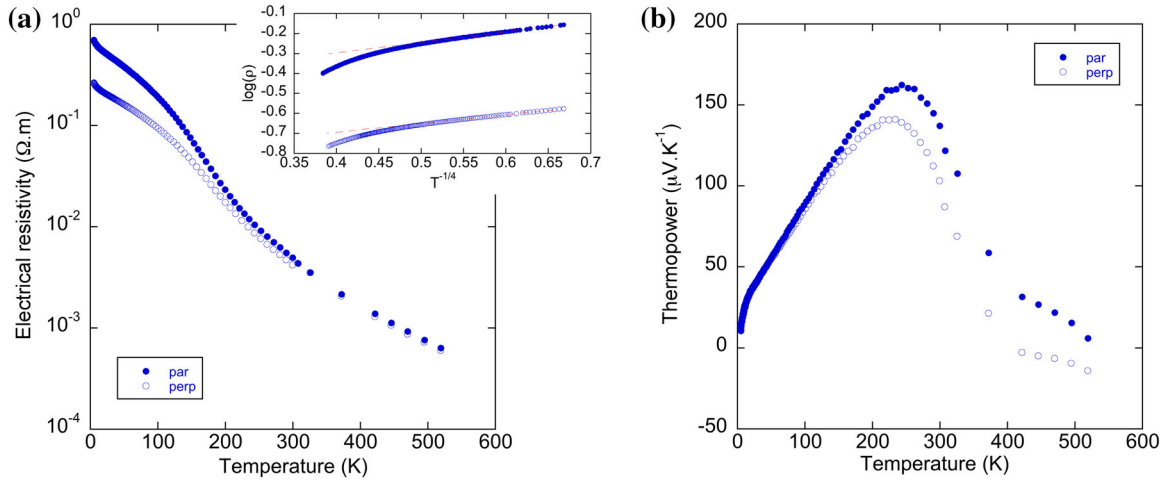

Fig. 5. Temperature dependence of the electrical resistivity ρ (a) and the Seebeck coefficient α (b) of the polycrystalline α-As_2Te_3 sample. The measurements performed parallel and perpendicular to the pressing direction are represented by filled and open symbols, respectively. Measurements at low (5 K–300 K) and high (300 K–523 K) temperature show great agreement at 300 K. The inset in (a) represents the evolution of ρ at low temperature in $T^{-1/4}$.

direction are displayed on Fig. 5a and b, respectively. Both properties exhibit a slight anisotropy, clearly observed below 200 K and above 150 K in the $\rho(T)$ and in the $\alpha(T)$, respectively. Over the entire temperature range, the electrical resistivity in both directions displays an activated behavior with values ranging from around 1 Ω m at 5 K to less than 600 μΩ m at 500 K. The high-temperature region can be described by an Arrhenius law $\rho = \rho_0 \cdot \exp[E_a/k_B T]$ (shown by the solid line in the inset of Fig. 5a), where the activation energy E_a = 65 meV, k_B the Boltzmann's constant and ρ_0 is a constant. This activation energy could imply an intrinsic semiconducting gap of ~130 meV. This result is however different from that of Sharma et al.,[11] deduced from ab-initio band structure calculations where a value of 400 meV was obtained. Below 17 K, ρ has a nearly exponential temperature dependence with a much lower activation energy. The best fit to the data in this temperature region was of the form $\rho = \rho_0 \cdot \exp[T_0/T]^{1/4}$ (where ρ_0 is a constant and T_0 is the characteristic temperature of the system) indicative of Mott variable range hopping.

$\alpha(T)$ does not evolve monotonically but increases with temperature up to 160 μV K^{-1} at 250 K, followed by a two-step decrease and a transition from *p*- to *n*-type transport above 400 K in the perpendicular direction only. This behavior is likely due to the manifestation of minority carriers effect (electrons in the present case). The fact that the *p*- to *n*-type transition is only seen in the perpendicular direction may point to some degree of anisotropy in the carrier mobility as well. Doping heavily this compound would result in pushing this transition towards higher temperatures and would likely enhance the power factor α^2/ρ. Comparisons between our results and the

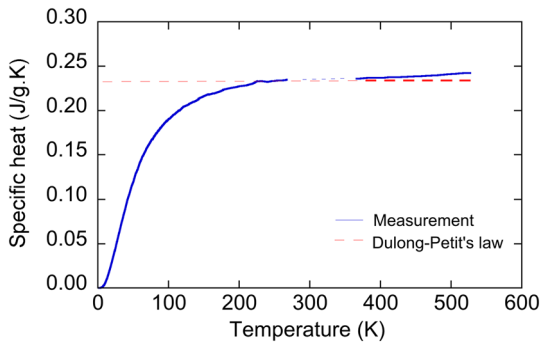

Fig. 6. Specific heat of the compound α-As_2Te_3 measured between 2 K and 260 K and between 360 K and 523 K. Between 260 K and 300 K, the influence of the addenda on the low-temperature measurement does not allow displaying reliable data. In the same fashion, measurement artifacts do not allow showing reliable data between 300 K and 360 K.

electronic transport properties predicted by band structure calculations show important deviations.[11] Among the possible reasons explaining these discrepancies, we speculate that the influence of native defects, not taken into account in the modeling, could play a major role. Actually, it is well-established that native defects such as anti-structure defects or vacancies can strongly affect the electronic transport properties in TE materials such as bismuth tellurides.[14] It is worth noticing that early studies showed *n*-type properties for the α-As_2Te_3 binary compound.[9,10] According to the EPMA measurements, the excess of Te in our material seems consistent with *p*-type conductivity, likely due to Te-doping on As sites as obtained by Harman[9] for α-As_2Te_3 single crystals with excess of Te.

Figure 6 displays the temperature dependence of the specific heat C_p. Extrapolation of the low temperature data is in very good agreement with the

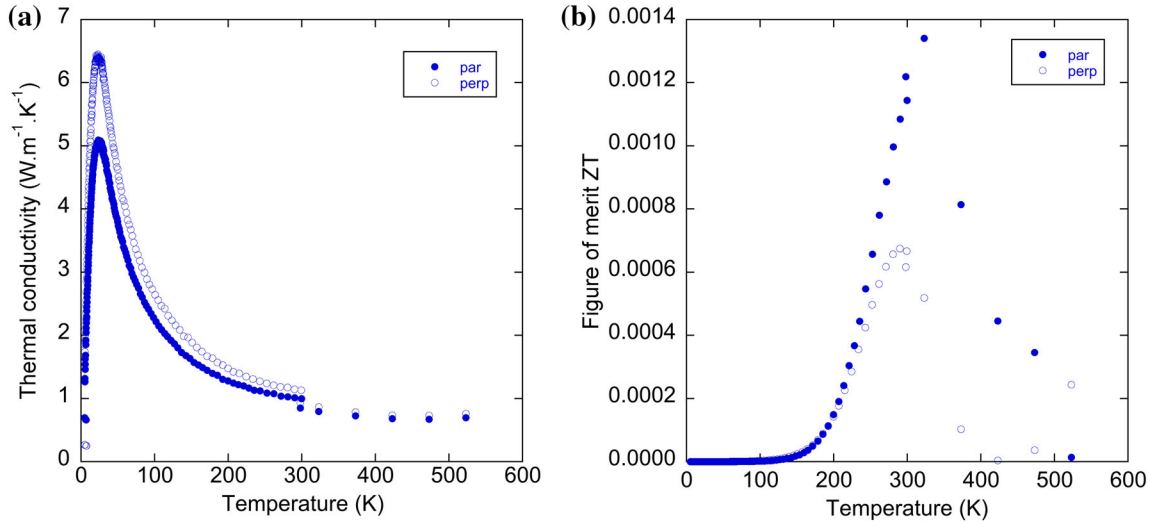

Fig. 7. Temperature-dependence of the thermal conductivity λ (a) and the figure of merit ZT (b) of the polycrystalline α-As_2Te_3 sample. The measurements performed parallel and perpendicular to the pressing direction are represented by filled and open symbols, respectively. The measurements of λ at low (5 K–300 K) and high (300 K–523 K) temperature show a slight discrepancy at 300 K due to issues in correcting the radiation heat loss over 200 K with the TTO option of the PPMS.

measurements above room temperature. It is seen that the specific heat deviates slightly from the calculated Dulong–Petit value of 0.234 J/g K between 300 K and 500 K. Figure 7a presents the temperature dependence of the thermal conductivity of α-As_2Te_3. λ shows a marked dielectric peak at low temperatures centered at 25 K, attaining the value of 6.5 W/m K in the perpendicular direction and 5.1 W/m K in the parallel direction, before decreasing to the very low value of 0.7 W m^{-1} K^{-1} at 523 K. Above 300 K, the anisotropy is no longer visible within experimental uncertainty. In this particular case, where the electrical resistivity is high, the electronic contribution to thermal conductivity is negligible, so that λ reflects exclusively the lattice contribution. Noteworthy, the thermal conductivity of β-As_2Te_3 is even lower, reaching values below 0.6 W m^{-1} K^{-1} at 423 K[4] with a non-negligible electronic contribution. In terms of ZT values, presented in Fig. 7b, the large electrical resistivity and the low thermopower values result in only very low ZT values around 0.001. Further studies aiming at probing the influence of different dopants are worthwhile to determine the potential of this compound for TE applications.

CONCLUSION

We presented results on the TE characterization of the compound α-As_2Te_3 between 5 K and 523 K. Owing to presumably low carrier concentration, the influence of minority carriers above 250 K strongly undermines the Seebeck coefficient, even leading to a sign change near 500 K. Even though displaying an interesting thermal conductivity lower than 1 W m^{-1} K^{-1} above 300 K, the very low power factors ($<5 \times 10^6$ W m^{-1} K^{-2}) therefore do not allow achieving high ZT values. However, this is not to say that this phase does not deserve further attention. Appropriate substitutions to tune the carrier concentration may be very beneficial into optimizing the ZT values.

REFERENCES

1. D.M. Rowe, *Thermoelectrics Handbook: Macro to Nano* (Boca Raton: CRC, 2006).
2. H.J. Goldsmid, *Thermoelectric Refrigeration* (New York: Plenum, 1964).
3. J. Snyder and E. Toberer, *Nat. Mater.* 7, 105 (2008).
4. J.B. Vaney, J. Carreaud, G. Delaizir, A. Pradel, A. Piarristeguy, C. Morin, E. Alleno, J. Monnier, A.P. Gonçalves, C. Candolfi, A. Dauscher, and B. Lenoir, *Adv. Electron. Mater.* 1, 1400008 (2015).
5. V.G. Yakushev and V.A. Kirinsky, *Doklady Akad Nauk SSSR* (1969), pp 882–884.
6. H.W. Shu, S. Jaulmes, and J. Flahaut, *Mater. Res. Bull.* 21, 1509 (1986).
7. S. Toscani, J. Dugué, R. Ollitrault, and R. Céolin, *Thermochim. Acta* 186, 247 (1991).
8. G. Carron, *Acta Crystallogr.* 16, 338 (1963).
9. T.C. Harman, B. Paris, S.E. Miller, and H.L. Goering, *J. Phys. Chem. Solids* 2, 181 (1957).
10. T.J. Scheidemantel, J.F. Meng, and J.V. Badding, *J. Phys. Chem. Solids* 66, 1744 (2005).
11. Y. Sharma, and P. Srivastava, *Opt. Mater.* 33, 899 (2011).
12. J.B. Vaney, G. Delaizir, E. Alleno, O. Rouleau, A. Piarristeguy, J. Monnier, C. Godart, M. Ribes, R. Escalier, A. Pradel, A.P. Goncalves, E.B. Lopes, G.J. Cuello, P. Ziolkowski, E. Muller, C. Candolfi, A. Dauscher, and B. Lenoir, *J. Mater. Chem. A* 1, 8190 (2013).
13. A. Stergiou, and P. Rentzeperis, *Z. Kristallogr.* 172(1–2), 139 (1985).
14. J.P. Fleurial, L. Gailliard, R. Triboulet, H. Scherrer, and S. Scherrer, *J. Phys. Chem. Solids* 49, 1237–1247 (1988).